

# Coverage Analysis for Dense Millimeter Wave Cellular Networks: The Impact of Array Size

Xianghao Yu\*, Jun Zhang\*, and K. B. Letaief\*<sup>†</sup>, *Fellow, IEEE*

\*Dept. of ECE, The Hong Kong University of Science and Technology, <sup>†</sup>Hamad Bin Khalifa University, Doha, Qatar

Email: \*{xyuam, eejzhang, eekhaled}@ust.hk, <sup>†</sup>kletaief@hbku.edu.qa

**Abstract**—Millimeter wave (mmWave) communications has been considered as a promising technology for 5G cellular networks. Exploiting directional beamforming using antenna arrays to combat path loss is one of the defining features in mmWave cellular networks. However, previous works on mmWave network analysis usually adopt simplified antenna patterns for tractability. In this paper, we show that there are huge discrepancies between the simplified and actual antenna patterns when investigating the coverage probability of mmWave networks. Analytical expressions for the coverage probabilities are derived using tools from stochastic geometry, by considering the actual antenna pattern with the uniform linear array. Moreover, the impact of the array size is investigated, which cannot be revealed from existing results with simplified antenna patterns. Numerical results will show that large-scale antenna arrays are required for satisfactory coverage in mmWave cellular networks. Furthermore, dense mmWave cellular networks are shown to achieve much higher rate coverage than conventional sub-6 GHz cellular systems.

## I. INTRODUCTION

To meet the ever-increasing demands for high-data-rate multimedia access, the capacity of next-generation wireless networks has to increase exponentially. One promising way to boost the capacity is to exploit new spectrum bands. Recently, millimeter wave (mmWave) bands from 30 GHz to 300 GHz have been proposed as a promising candidate for new spectrum in 5G cellular networks, which previously are only considered for indoor and fixed outdoor scenarios [1].

Highly directional antenna arrays at the transceivers can compensate for the additional free space path loss caused by the ten-fold increase of the carrier frequency in mmWave systems [2]. Recently, channel measurements using directional antenna arrays have revealed some unique propagation characteristics of mmWave signals [3]. It turns out that mmWave signals are sensitive to blockages, which causes totally different path loss laws for the line-of-sight (LOS) and non-line-of-sight (NLOS) mmWave signals. In addition, dense deployments are required to relieve the signal interception in mmWave cellular networks due to the blockage sensitivity, which, fortunately, fits the evolution of network densification, e.g., by deploying small cells [4].

More importantly, combined with the poor scattering environment, directional antennas will dramatically change the signal power, as well as the interference power. In mmWave cellular networks, the received signal or interference power is closely related to the angles of departure/arrival (AoDs/AoAs).

In particular, the antenna array will provide various power gains corresponding to different AoDs/AoAs. A slight shift of AoD/AoA may lead to a large array gain variation when directional antenna arrays are used. Therefore, it is necessary and critical to incorporate the impact of antenna arrays when analyzing mmWave cellular networks.

To maintain analytical tractability, the antenna patterns are often simplified in previous analysis of mmWave systems, with the *flat-top* pattern being a widely used approximation. Since the directional antenna array is one of the differentiating features in mmWave cellular systems, it is intriguing to evaluate its influence on the network performance. However, it is difficult to depict the impact of antenna arrays when using simplified antenna patterns. In practice, some critical parameters of the antenna beam pattern such as beamwidth, the  $n$ th minor lobe maxima, nulls, and front-back ratio are all determined by the array size. With simplified antenna patterns, these parameters can only be determined qualitatively and inaccurately according to the array size. Hence, the simplification of the antenna pattern results in some difficulty and inaccuracy when analyzing the performance of mmWave cellular systems.

There exist several previous studies on performance analysis for mmWave networks [5]–[9]. In [5]–[8], analytical results on signal-to-interference-plus-noise ratio (SINR) and rate coverage based on the flat-top pattern were obtained. Moreover, the channel model was also simplified and did not reflect the propagation characteristics of mmWave systems. The actual antenna pattern was adopted in [9] for evaluating the capacity of an interfered communication link. Nevertheless, all the interferers were assumed to use the same array gain, which weakened the practicality of the result.

In this paper, we first demonstrate that the difference between the simplified and actual antenna patterns will introduce considerable discrepancies between the theoretical and practical results. We will then investigate the coverage probability in the downlink mmWave cellular network with a random spatial network model, where base stations (BSs) are modeled as a homogeneous Poisson point process (PPP). We assume that the BSs adopt analog beamforming to serve the users and we retain the actual antenna pattern in our work, which is different from prior works and forms the main challenge for analysis in the meantime. Based on some reasonable approximations, we derive a tractable expression of the coverage probability for dense mmWave networks, which contains a single integral operation, and can be easily and efficiently computed. Based on the analytical results, the impacts of antenna array sizes are investigated. It will be shown that large-

This work was supported by the Hong Kong Research Grants Council under Grant No. 610113.

scale antenna arrays are needed in mmWave cellular networks to maintain an acceptable coverage probability. A comparison between mmWave cellular networks and conventional sub-6 GHz systems will also be provided, and shall demonstrate the superiority of mmWave networks.

## II. SYSTEM MODEL

In this section, we will first describe the random spatial network model and blockage model for mmWave cellular networks. Afterwards, we will present the mmWave channel model.

### A. Network Model

We consider a mmWave cellular network, where BSs and users are distributed according to two independent homogeneous PPPs [10]. Since the user process is stationary and independent of the BS process, the downlink SINR of the typical user has the same distribution as the aggregate ones in the network [10]. We assume that each user has a single receive antenna, and is served by the nearest BS equipped with a directional antenna array composed of  $N_t$  elements. All BSs are assumed to transmit with the same transmit power  $P_t$ , and each BS will serve the users in a round-robin fashion, i.e., intracell time division multiple access (TDMA) is adopted in this paper.

We introduce the *LOS ball* to model the blockage as shown in Fig. 1, and it has been shown to be accurate in dense mmWave cellular networks [5]. In this blockage model, we define a LOS radius  $R$ , which symbolizes the average distance between a user and its nearby blockages, and therefore the LOS probability of a certain link is one within  $R$  and zero outside the radius. The incorporation of the blockage effects induces different path loss laws for LOS and NLOS links. It turns out that NLOS interferers are negligible under dense BS deployments. In other words, dense mmWave networks are *LOS interference limited*. Hence, we will focus on the interference brought by the LOS interferers, whose spatial distribution is a PPP, denoted as  $\Phi$  with density  $\lambda$ , in a finite area with radius  $R$ . Later we will justify this assumption through simulation in Section V.

Directional antenna arrays are leveraged to provide significant beamforming gains to overcome the path loss and to synthesize highly directional beams. The received signal for a typical user, denoted as the 0th user, is given by

$$y_0 = \sqrt{\beta} r^{-\frac{\alpha}{2}} \mathbf{h}_0 \mathbf{w}_0 \sqrt{P_t} s_0 + \sum_{i \neq 0} \sqrt{\beta} R_i^{-\frac{\alpha}{2}} \mathbf{h}_i \mathbf{w}_i \sqrt{P_t} s_i + n_0, \quad (1)$$

where  $r$  is the distance between the serving BS and the typical user, while  $R_i$  is the distance between  $i$ th BS and the typical user. A  $1 \times N_t$  vector  $\mathbf{h}_i$  is used to denote the small scale fading between the  $i$ th BS and the typical user, and the path loss exponent and intercept are  $\alpha$  and  $\beta$ , respectively. In addition, the beamforming vector of the  $i$ th BS is denoted as  $\mathbf{w}_i$ , and  $n_0$  stands for the additive white Gaussian noise (AWGN).

### B. Channel Model

Due to high free-space path loss, the mmWave propagation environment is well characterized by a clustered channel

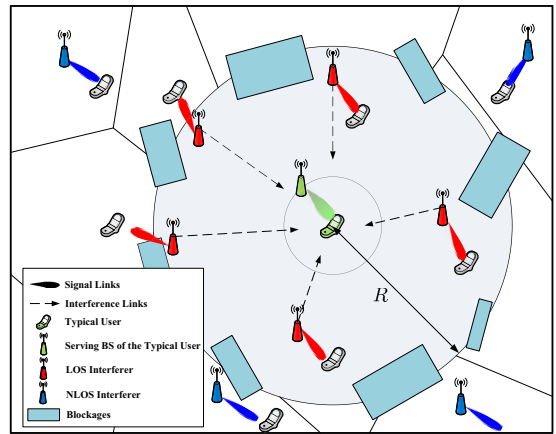


Fig. 1. A sample network model where BSs and users are modeled as two independent PPPs, and each user is associated with the nearest BS. The LOS ball is used to model the blockages in the network.

model, i.e., the Saleh-Valenzuela model [3], which can be depicted as

$$\mathbf{h}_i = \sqrt{N_t} \sum_{l=1}^L \alpha_{il} \mathbf{a}_t^H(\theta_{il}), \quad (2)$$

where  $(\cdot)^H$  symbolizes the conjugate transpose, and  $L$  is the number of clusters. The gain of the  $l$ th cluster is denoted as  $\alpha_{il}$ , which follows independent Nakagami fading for each link [5]. For mmWave channels containing LOS components, the effect of NLOS signals is marginal since the channel gains of NLOS paths are typically 20 dB weaker than those of LOS signals [3]. Hence, for the remainder of this paper, we will focus on the LOS path, i.e.,  $L = 1$ . In addition,  $\mathbf{a}_t(\theta_i)$  represent the transmit array response vectors corresponding to the AoDs  $\theta_i$ , which are independent and identically distributed (i.i.d.) according to a uniform distribution on the interval  $[0, 2\pi]$  [3]. In this paper, we consider the uniform linear array (ULA) with  $N_t$  antenna elements. Therefore, the array response vectors can be written as

$$\mathbf{a}_t(\theta_i) = \frac{1}{\sqrt{N_t}} \left[ 1, \dots, e^{jkdx \cos \theta_i}, \dots, e^{jk d(N_t-1) \cos \theta_i} \right]^T, \quad (3)$$

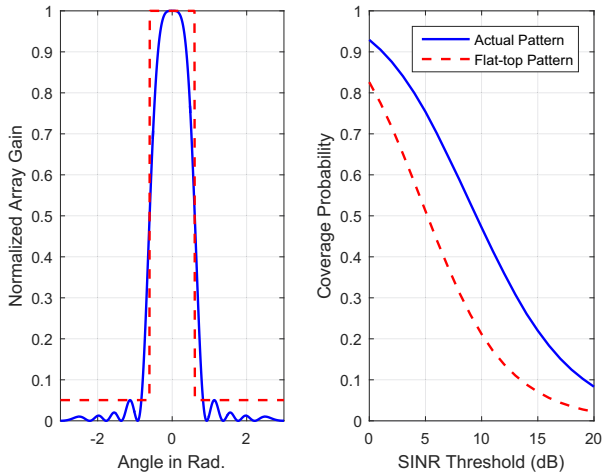
where  $d$  and  $k$  are the antenna spacing and wavenumber, and  $0 \leq x < N_t$  is the antenna index. In order to enhance the directionality of the beam, the antenna spacing  $d$  should be less than half-wavelength to avoid grating lobes [11].

## III. ANALOG BEAMFORMING AND ANTENNA PATTERN

In this section, we will first introduce the optimal analog beamforming strategy and then illustrate the necessity of employing the actual antenna pattern when analyzing mmWave cellular networks.

### A. Analog Beamforming

While various space-time processing techniques can be applied at each multi-antenna mmWave BS, we will focus on the analog beamforming, which is able to control the beam direction via phase shifters. Due to the low cost and power consumption, analog beamforming has already been used in



(a) Visualization of two different antenna patterns. (b) Coverage probability evaluation using two different antenna patterns.

Fig. 2. The comparison between the flat-top pattern and the actual pattern.

some mmWave systems such as WiGig (IEEE 802.11ad) [1]. Assuming the AoD of the channel between the  $i$ th BS and its serving user is  $\phi_i$ , the optimal analog beamforming vector is

$$\mathbf{w}_i = \mathbf{a}_t(\phi_i), \quad (4)$$

which means the BS should align the beam direction exactly with the AoD of the channel to obtain the maximum power gain.

### B. Antenna Pattern

Based on the optimal analog beamforming vector (4), for the typical user, the power gain provided by the small scale fading and beamforming of the  $i$ th BS can be expressed as

$$|\mathbf{h}_i \mathbf{w}_i|^2 = N_t |\alpha_i|^2 |\mathbf{a}_t^H(\theta_i) \mathbf{a}_t(\phi_i)|^2 \triangleq N_t g_i G(\theta_i, \phi_i), \quad (5)$$

where  $g_i$  is the power gain of small scale fading and  $G(\theta_i, \phi_i)$  is the normalized array gain of the  $i$ th BS, which can be expressed as

$$\begin{aligned} G(\theta_i, \phi_i) &= |\mathbf{a}_t^H(\theta_i) \mathbf{a}_t(\phi_i)|^2 \\ &= \frac{1}{N_t^2} \left| \sum_{x=0}^{N_t-1} e^{jkdx(\cos \theta_i - \cos \phi_i)} \right|^2 \\ &= \frac{\sin^2 \left[ \frac{N_t}{2} kd(\cos \theta_i - \cos \phi_i) \right]}{N_t^2 \sin^2 \left[ \frac{1}{2} kd(\cos \theta_i - \cos \phi_i) \right]}. \end{aligned} \quad (6)$$

The flat-top pattern is often used as an approximation of the actual antenna pattern, where the array gains within the half-power beamwidth (HPBW) [11] are assumed to be the maximum power gain and the array gains corresponding to the remaining AoDs are approximated to be the first minor maximum gain of the actual pattern, as shown in Fig. 2(a) [5]. However, this approximation will introduce huge discrepancies when we evaluate the network coverage probability. A simulation result<sup>1</sup> in Fig. 2(b) shows that there is a large gap between the SINR coverage probabilities using two different antenna patterns.

<sup>1</sup>The parameter setting is the same as that of Fig. 4 in Section V.

More importantly, given the operating frequency and the antenna spacing, the antenna pattern is critically determined by the array size. In the flat-top pattern, however, it is very difficult to quantitatively and accurately depict the variation of the HPBW and the first minor maximum for different array sizes and AoDs. In other words, the simplified antenna patterns obliterate the possibility of analyzing the impact of directional antenna arrays, which is a critical and unique issue in mmWave systems. Hence, it is necessary to retain the actual antenna pattern in the analysis of mmWave cellular networks, in order to investigate the role of the antenna array in mmWave networks and to ensure the consistency with practical systems.

## IV. COVERAGE ANALYSIS

In this section, we will derive a tractable expression for the coverage probability considering the actual antenna pattern. The bottleneck of the analysis is the distribution of the interference power due to the complicated form of the normalized array gain  $G(\theta_i, \phi_i)$ . Based on some approximations, we will provide an analytical result which can be easily evaluated.

### A. Signal-to-interference-plus-noise Ratio

We assume that each BS has full information about the AoD of the channel between itself and its serving user, and can align the beam to the AoD direction using analog beamforming. From (1)-(6), the receive SINR is given by

$$\begin{aligned} \text{SINR} &= \frac{P_t N_t |\alpha_0|^2 |\mathbf{a}_t^H(\theta_0) \mathbf{w}_0|^2 \beta r^{-\alpha}}{\sigma^2 + \sum_{i \in \Phi \setminus 0} P_t N_t |\alpha_i|^2 |\mathbf{a}_t^H(\theta_i) \mathbf{w}_i|^2 \beta R_i^{-\alpha}} \\ &= \frac{g_0 r^{-\alpha}}{\sigma_n^2 + \sum_{i \in \Phi \setminus 0} g_i G(\theta_i, \phi_i) R_i^{-\alpha}} \triangleq \frac{g_0 r^{-\alpha}}{\sigma_n^2 + I}, \end{aligned} \quad (7)$$

where  $g_i$  is a Gamma distributed random variable according to the Nakagami fading assumption, and  $\sigma_n^2 = \frac{\sigma^2}{\beta P_t N_t}$  is the normalized noise. In this paper, we will evaluate the coverage probability, which is defined as the probability that the received SINR is greater than a given threshold  $\gamma$ , i.e.,

$$p_c(\gamma) = \mathbb{P}(\text{SINR} > \gamma), \quad (8)$$

where SINR is given in (7).

### B. Analysis of Coverage Probability

Since we assume that each user is served by the nearest BS and the PPP  $\Phi$  is in a finite area with radius  $R$ , the conditional distribution of the distance  $r$  between the serving BS and the typical user is

$$f(r) = \frac{2\pi\lambda r}{1 - e^{-\lambda\pi R^2}} e^{-\pi\lambda r^2}, \quad (9)$$

and for dense networks, we have  $e^{-\lambda\pi R^2} \approx 0$ . Based on (7) and (8), the coverage probability is given by

$$p_c(\gamma) = \int_0^R f(r) \mathbb{P}[g_0 > \gamma r^\alpha (\sigma_n^2 + I)] dr, \quad (10)$$

where  $g_0$  is a normalized gamma random variable with the Nakagami fading parameter  $N$ .

$$\mathcal{I}(r) = \begin{cases} r \exp \left[ -\xi n \gamma \sigma_n^2 r^\alpha - \pi \lambda r^2 + \frac{4\pi^2 \lambda e^\alpha}{kdAN_t} \sum_{p=1}^{\infty} \frac{(-1)^p}{p!} \sum_{q=1}^p (R^{2-\alpha q} r^{\alpha q} - r^2) I(p, q) \right] & \alpha \neq 2 \\ r \exp \left[ -\xi n \gamma \sigma_n^2 r^2 - \pi \lambda r^2 + \frac{2\pi^2 \lambda \xi n \gamma (\ln r - \ln R)}{kdAN_t} r^2 + \frac{4\pi^2 \lambda e^\alpha}{kdAN_t} \sum_{p=2}^{\infty} \frac{(-1)^p}{p!} \sum_{q=2}^p (R^{2-2q} r^{2q} - r^2) I(p, q) \right] & \alpha = 2 \end{cases} \quad (20)$$

**Lemma 1.** (From [12]) For a normalized gamma random variable  $g$  with parameter  $N$ , the probability  $\mathbb{P}(g < \gamma)$  can be tightly upper bounded by

$$\mathbb{P}(g < \gamma) < (1 - e^{-\xi \gamma})^N, \quad (11)$$

where  $\xi = N(N!)^{-\frac{1}{N}}$ .

Based on Lemma 1, a tight lower bound of the probability  $\mathbb{P}[g_0 > \gamma r^\alpha (\sigma_n^2 + I)]$  can be derived as<sup>2</sup>

$$\begin{aligned} & \mathbb{P}[g_0 > \gamma r^\alpha (\sigma_n^2 + I)] \\ & > 1 - \mathbb{E}_I \left[ \left( 1 - e^{-\xi \gamma r^\alpha (\sigma_n^2 + I)} \right)^N \right] \\ & = \sum_{n=1}^N (-1)^{n+1} \binom{N}{n} e^{-\xi n \gamma r^\alpha \sigma_n^2} \mathcal{L}_I(\xi n \gamma r^\alpha). \end{aligned} \quad (12)$$

It can be seen from (12) that the main task to obtain the coverage probability  $p_c(\gamma)$  is to derive the Laplace transformation of the interference  $\mathcal{L}_I(s)$ , which can be further derived as<sup>3</sup>

$$\begin{aligned} \mathcal{L}_I(s) & \stackrel{(a)}{=} \exp \left\{ -2\pi \lambda \int_r^R (1 - \mathbb{E}_{g_i, G_i}[\exp(-s g_i G_i x^{-\alpha})]) x dx \right\} \\ & \stackrel{(b)}{\geq} \exp \left\{ -2\pi \lambda \int_r^R (1 - \mathbb{E}_{G_i}[\exp(-s G_i x^{-\alpha})]) x dx \right\}, \end{aligned} \quad (13)$$

where (a) follows the Laplace functional of the PPP  $\Phi$ , and (b) follows the Jensen's inequality. One intuitive way to manipulate the moment-generating function with respect to the array gain in (13) is to directly derive the distribution of the array gain. However, this is highly intractable due to the complicated form of (6). We will next give an analytical result based on some reasonable approximations.

*Approximation 1:* We approximate the denominator of the array gain function as  $N_t^2 \left[ \frac{1}{2} kd(\cos \theta_i - \cos \phi_i) \right]^2$ . In (6), the antenna spacing should be less than half-wavelength. Therefore, the term  $\frac{1}{2} kd(\cos \theta_i - \cos \phi_i)$  should be within a small range near zero, and the approximation is established due to the fact that  $\sin x \approx x$  when  $x$  is small.

*Approximation 2:* The distribution of the random variable  $\cos \theta_i - \cos \phi_i$  cannot be expressed in a closed-form, which is the main obstacle for further analysis. Here, we propose to use a uniform distribution in  $[-A, A]$  to approximate the original distribution. Although this approximation is heuristic, to some extent, it creates the possibility to analyze the coverage probability with the actual antenna pattern, and the accuracy will be tested through simulation in Section V.

<sup>2</sup>Lemma 1 also gives a tight lower bound of the coverage probability in (10).

<sup>3</sup>The array gain  $G(\theta_i, \phi_i)$  is abbreviated as  $G_i$  for notational simplicity.

Based on Approximations 1 and 2, the array gain (6) is approximated as the square of a sinc function with respect to a uniformly distributed variable  $\varphi_i$  as follows

$$G(\varphi_i) \approx \frac{\sin^2 \left( \frac{N_t}{2} kd \varphi_i \right)}{\left( \frac{N_t}{2} kd \varphi_i \right)^2}. \quad (14)$$

**Lemma 2.** The definite integral from 0 to  $\infty$  of the  $q$ -th power of the squared sinc function is given by

$$\int_0^\infty \frac{\sin^{2q} \varphi}{\varphi^{2q}} d\varphi = q\pi \sum_{k=0}^q \frac{(-1)^k (q-k)^{2q-1}}{k!(2q-k)!}. \quad (15)$$

*Proof:* Through Euler's formula and the binomial theorem, the original integral can be manipulated as

$$\lim_{\epsilon \rightarrow 0^+} \frac{1}{2} \frac{1}{(2j)^{2q}} \sum_{k=0}^{2q} (-1)^k \binom{2q}{k} \int_{-\infty}^{\infty} \frac{e^{j\varphi 2(q-k)}}{(x-j\epsilon)^q} d\varphi. \quad (16)$$

According to the residue theorem and Cauchy differentiation formula, we find the original integral equals

$$\frac{1}{2} \frac{1}{(2j)^{2q}} \sum_{k=0}^q (-1)^k \binom{2q}{k} \frac{2\pi j}{(2q-1)!} \frac{d^{2q-1}}{d\varphi^{2q-1}} e^{j\varphi 2(q-k)}, \quad (17)$$

which can be simplified as (15).  $\blacksquare$

Based on Lemma 2 and (14), we can tackle the moment-generating function in (13), which is the bottleneck of the analysis.

**Lemma 3.** The moment-generating function with respect to the array gain  $\mathbb{E}_{G_i}[\exp(-s G_i x^{-\alpha})]$  can be expressed as

$$\begin{aligned} & \mathbb{E}_{G_i}[\exp(-s G_i x^{-\alpha})] \\ & \approx 1 + \frac{2\pi e^\alpha}{kdAN_t} \sum_{p=1}^{\infty} \frac{(-1)^p}{p!} \sum_{q=1}^p \binom{p}{q} s^q \times \\ & \quad x^{-\alpha q} a^{p-q} q \sum_{k=0}^q \frac{(-1)^k (q-k)^{2q-1}}{k!(2q-k)!}. \end{aligned} \quad (18)$$

*Proof:* See Appendix A.  $\blacksquare$

Now, with Lemma 3, we present the main result on the SINR coverage probability  $p_c(\gamma)$  as follows.

**Theorem 1.** The SINR coverage probability  $p_c(\gamma)$  can be computed as

$$p_c(\gamma) \approx \frac{2\pi \lambda}{1 - e^{-\lambda \pi R^2}} \sum_{n=1}^N (-1)^{n+1} \binom{N}{n} \int_0^R \mathcal{I}(r) dr, \quad (19)$$

where  $\mathcal{I}(r)$  is given by (20) and

$$I(p, q) = \binom{p}{q} \frac{(\xi n \gamma)^q a^{p-q} q}{2 - \alpha q} \sum_{k=0}^q \frac{(-1)^k (q-k)^{2q-1}}{k!(2q-k)!}. \quad (21)$$

*Proof:* The proof is established by applying Lemma 3 to (13) with some basic manipulations on integral operations and then substituting into (9), (10), and (12). ■

*Remark 1:* The analytical result of the coverage probability given in (19) can be easily evaluated by numerical integration. Although (20) involves a summation of infinite terms, it will be shown in Section V that the high-order terms contribute little to the whole summation, and using finite terms is accurate enough for numerical computation. Furthermore, a proper choice of the parameter  $a$  at which the series expands will save the number of terms to be calculated.

## V. NUMERICAL RESULTS

In this section, we will first examine the approximation made in Section IV. We will then demonstrate our result through simulations. We assume that the bandwidth is 500 MHz, and the transmit power of all the BSs is set to 1 Watt. The separation between the antenna elements is quarter-wavelength to avoid grating lobes. From the recent measurements of LOS mmWave signal propagations [3], the path loss exponent  $\alpha$  is equal to or slightly larger than two and  $\beta = -61.4$  dB. All simulation results are averaged over 500 thousand realizations.

### A. Justification of Approximation 2

In Approximation 2, we proposed to approximate the distribution of  $\cos \theta_i - \cos \phi_i$  as a uniform distribution. Here we will justify this approximation through evaluating the cumulative distribution functions of  $G(\theta_i, \phi_i)$  in (6) and  $G(\varphi_i)$  in (14). We approximate the parameter in uniform distribution  $A = 0.8$ , and this value will be used in all the following numerical evaluations.

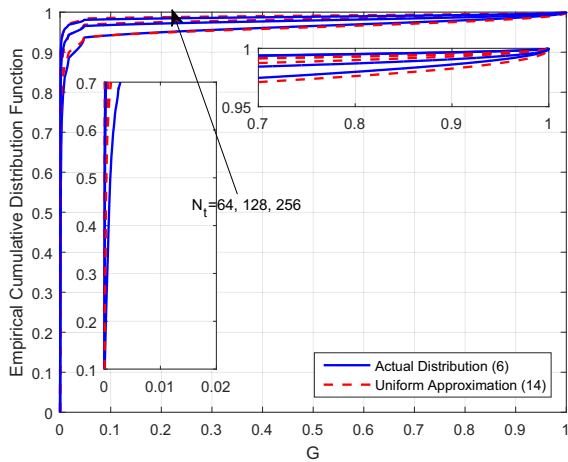


Fig. 3. The cumulative distribution functions of  $G(\theta_i, \phi_i)$  in (6) and  $G(\varphi_i)$  in (14).

From Fig. 3, we can see that, based on Approximation 2, two cumulative distribution functions almost coincide with each other. It indicates that the distributions of two array gains are almost the same. This justifies that Approximation 2 is reasonable in the sense of the distribution of array gains, which is the critical part in the analysis.

### B. Coverage Probability Evaluation

We shall now provide the simulation results to verify the analytical result in Section IV. The Nakagami fading parameter  $N$  is set to 2, and the path loss exponent is  $\alpha = 2$ . We compare the simulation results and the analytical results from Theorem 1. To verify the assumption that mmWave networks are LOS interference limited, we also include the NLOS BSs in the simulation, where we assume that  $N = 1$ , i.e., Rayleigh fading,  $\beta_n = -72$  dB, and the path loss exponent  $\alpha = 4$  for the NLOS interfering signals.

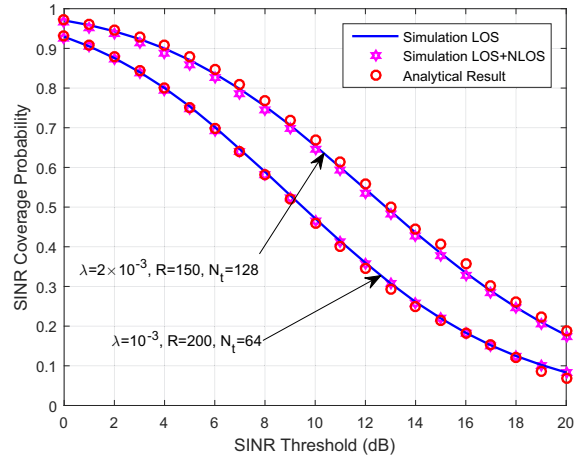


Fig. 4. SINR coverage probability in dense mmWave cellular networks with different parameter settings.

Fig. 4 verifies that dense mmWave cellular networks are indeed LOS interference limited, which means that the NLOS interference is small compared to the total interference due to the more severe path loss and small scale fading. When we numerically calculate (19) in Theorem 1, a finite number of terms are included in the summation, as illustrated in Remark 1, until the numerical values converge. We propose to set  $a = -\xi n \gamma / 2$  to save the number of the terms involved in the summation. Fig. 4 also shows that the approximations and the derivations in Section IV are reasonable and accurate for different settings of the network, so the coverage probability  $p_c(\gamma)$  provided in Theorem 1 can be regarded as a reliable analytical result when considering the directional antenna pattern in mmWave cellular networks.

### C. Impact of Array Size

In this subsection, we will investigate the impact of directional antenna arrays and compare mmWave cellular systems with conventional sub-6 GHz ones. In mmWave networks, we assume that the LOS radius is 200 meters, the Nakagami fading parameter  $N = 3$ , and the path loss exponent  $\alpha = 2.1$ . In conventional networks, we assume that small scale fading is i.i.d. Rayleigh fading and the path loss exponent equals 4. All BSs use maximum ratio transmission beamforming to transmit a single data stream with 100 MHz available bandwidth. For both systems, we assume a dense BS deployment with density of  $1 \times 10^{-3}$  BSs per unit area, and evaluate the rate coverage probability with the antenna array size from 64 to 256.

The rate coverage probability is defined as  $\mathbb{P}[W \log_2(1 + \text{SINR}) > \hat{\gamma}] = p_c(2^{\hat{\gamma}/W} - 1)$ , where  $W$  is the bandwidth

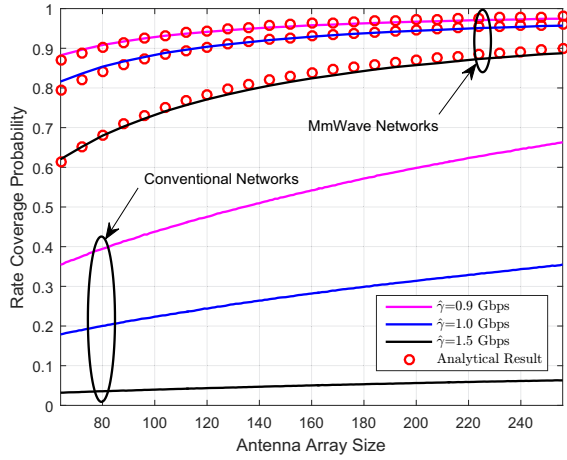


Fig. 5. Rate coverage probability in dense mmWave cellular networks with different parameter settings.

and  $\hat{\gamma}$  is the rate threshold. The results in Fig. 5 show that, for a given rate requirement, large-scale antenna arrays are needed in mmWave cellular networks to guarantee an acceptable coverage probability. It also shows that the coverage probability of conventional systems is much lower than that of mmWave networks. This phenomenon shows that the large bandwidth and directional antenna arrays benefit mmWave systems. Moreover, as it is much easier to implement large-scale antenna arrays in mmWave systems than conventional ones, thanks to the small wavelength, mmWave networks stand out as an excellent candidate for future 5G systems to provide multi-gigabits per second data rate.

## VI. CONCLUSIONS

One main contribution of this paper was identifying the importance of using the actual antenna pattern in the coverage analysis for mmWave networks. In particular, it was demonstrated that the widely used flat-top antenna pattern will result in a large performance gap compared to practical systems. On the contrary, with the actual antenna pattern, we were able to investigate the impact of the array size on the coverage probability. Numerical results showed that large-scale directional antenna arrays are needed in mmWave cellular systems to guarantee an acceptable coverage probability. MmWave cellular networks, taking advantage of the wide bandwidth and exploiting directional transmission, were shown to achieve a much higher rate coverage than conventional sub-6 GHz networks. It will be interesting to extend the coverage analysis to mmWave cellular networks with more advanced precoding techniques, e.g., hybrid precoding [13], [14], which can support spatial multiplexing.

## APPENDIX A PROOF OF LEMMA 2

Based on the approximated array gain (14), we can derive the moment-generating function as

$$\stackrel{(c)}{=} \mathbb{E}_{G_i} [\exp(-sG_i x^{-\alpha})] \\ = \frac{e^a}{2A} \int_{-A}^A \left\{ \sum_{p=0}^{\infty} \frac{1}{p!} \left[ -sx^{-\alpha} \frac{\sin^2\left(\frac{N_t}{2}kd\varphi_i\right)}{\left(\frac{N_t}{2}kd\varphi_i\right)^2} - a \right]^p \right\} d\varphi_i, \quad (22)$$

where (c) follows the series expansion of the exponential function at point  $a$ . Then switching the order of the integral and summation, we can find that (22) is equal to

$$\frac{e^a}{A} \sum_{p=0}^{\infty} \frac{(-1)^p}{p!} \left[ Aa^p + \sum_{q=1}^p \binom{p}{q} s^q \times \right. \\ \left. x^{-\alpha q} a^{p-q} \int_0^A \frac{\sin^{2q}\left(\frac{N_t}{2}kd\varphi_i\right)}{\left(\frac{N_t}{2}kd\varphi_i\right)^{2q}} d\varphi_i \right] \quad (23) \\ \stackrel{(d)}{<} \frac{e^a}{A} \sum_{p=0}^{\infty} \frac{(-1)^p}{p!} \left[ Aa^p + \sum_{q=1}^p \binom{p}{q} s^q \times \right. \\ \left. x^{-\alpha q} a^{p-q} \frac{2q\pi}{kdN_t} \sum_{k=0}^q \frac{(-1)^k (q-k)^{2q-1}}{k!(2q-k)!} \right],$$

which gives the expression in (18), and (d) follows Lemma 2 given that, for the tails of the  $2q$ -th power of the sinc function, the integrals are negligible when  $N_t$  is not too small.

## REFERENCES

- [1] E. Perahia, C. Cordeiro, M. Park, and L. Yang, "IEEE 802.11ad: Defining the next generation multi-Gbps Wi-Fi," in *Proc. 2010 7th IEEE Consumer Commun. and Netw. Conf. (CCNC)*, Jan. 2010, pp. 1–5.
- [2] G. R. MacCartney, M. K. Samimi, and T. S. Rappaport, "Exploiting directionality for millimeter-wave wireless system improvement," in *Proc. 2015 IEEE Int. Conf. Commun. (ICC)*, London, UK, June 2015, pp. 2416–2422.
- [3] M. Akdeniz, Y. Liu, M. Samimi, S. Sun, S. Rangan, T. Rappaport, and E. Erkip, "Millimeter wave channel modeling and cellular capacity evaluation," *IEEE J. Sel. Areas Commun.*, vol. 32, no. 6, pp. 1164–1179, June 2014.
- [4] C. Li, J. Zhang, and K. B. Letaief, "Throughput and energy efficiency analysis of small cell networks with multi-antenna base stations," *IEEE Trans. Wireless Commun.*, vol. 13, no. 5, pp. 2505–2517, May 2014.
- [5] T. Bai and R. W. Heath, "Coverage and rate analysis for millimeter-wave cellular networks," *IEEE Trans. Wireless Commun.*, vol. 14, no. 2, pp. 1100–1114, Feb. 2015.
- [6] M. Kulkarni, S. Singh, and J. Andrews, "Coverage and rate trends in dense urban mmwave cellular networks," in *Proc. 2014 IEEE Global Commun. Conf. (GLOBECOM)*, Austin, TX, Dec. 2014, pp. 3809–3814.
- [7] A. Thornburg, T. Bai, and R. W. Heath, "Mmwave ad hoc network coverage and capacity," in *Proc. 2015 IEEE Int. Conf. Commun. (ICC)*, London, UK, June 2015, pp. 1310–1315.
- [8] K. Venugopal, M. C. Valenti, and R. W. Heath, "Interference in finite-sized highly dense millimeter wave networks," in *Proc. 2015 Inf. Theory and Appl. (ITA)*, San Diego, CA, Feb. 2015, pp. 175–180.
- [9] F. Babich and M. Comisso, "A reliable approach for modeling the actual antenna pattern in millimeter-wave communication," *IEEE Commun. Lett.*, vol. 19, no. 8, pp. 1335–1338, Aug. 2015.
- [10] M. Haenggi, *Stochastic Geometry for Wireless Networks*. Cambridge University Press, 2012.
- [11] C. A. Balanis, *Antenna Theory: Analysis and Design*. John Wiley & Sons, 2005.
- [12] H. Alzer, "On some inequalities for the incomplete Gamma function," *Math. Comput.*, vol. 66, no. 218, pp. 771–778, Apr. 1997.
- [13] O. El Ayach, S. Rajagopal, S. Abu-Surra, Z. Pi, and R. W. Heath, "Spatially sparse precoding in millimeter wave MIMO systems," *IEEE Trans. Wireless Commun.*, vol. 13, no. 3, pp. 1499–1513, Mar. 2014.
- [14] X. Yu, J.-C. Shen, J. Zhang, and K. B. Letaief, "Alternating minimization algorithms for hybrid precoding in millimeter wave MIMO systems," *IEEE J. Sel. Topics Signal Process.*, to appear.